Published in final edited form as:
Langmuir. 2012 January 24; 28(3): 1931–1941. doi:10.1021/la204399m.

Control of initiation, rate, and routing of spontaneous capillary-driven flow of liquid droplets through microfluidic channels on SlipChip

Rebecca R. Pompano[1], **Carol E. Platt**[1], **Mikhail A. Karymov**[2], and **Rustem F. Ismagilov**[2]

[1] Department of Chemistry and Institute for Biophysical Dynamics, The University of Chicago, 929 E. 57th St, Chicago, IL 60637

[2] Division of Chemistry and Chemical Engineering, California Institute of Technology, 1200 E. California Blvd, Pasadena, CA 91125

Abstract

This paper describes the use of capillary pressure to initiate and control the rate of spontaneous liquid-liquid flow through microfluidic channels. In contrast to flow driven by external pressure, flow driven by capillary pressure is dominated by interfacial phenomena and is exquisitely sensitive to the chemical composition and geometry of the fluids and channels. A step-wise change in capillary force was initiated on a hydrophobic SlipChip by slipping a shallow channel containing an aqueous droplet into contact with a slightly deeper channel filled with immiscible oil. This action induced spontaneous flow of the droplet into the deeper channel. A model predicting the rate of spontaneous flow was developed based on the balance of net capillary force with viscous flow resistance, using as inputs the liquid-liquid surface tension, the advancing and receding contact angles at the three-phase aqueous-oil-surface contact line, and the geometry of the devices. The impact of contact angle hysteresis, the presence or absence of a lubricating oil layer, and adsorption of surface-active compounds at liquid-liquid or liquid-solid interfaces were quantified. Two regimes of flow spanning a 10^4-fold range of flow rates were obtained and modeled quantitatively, with faster (mm/s) flow obtained when oil could escape through connected channels as it was displaced by flowing aqueous solution, and slower (micrometer/s) flow obtained when oil escape was mostly restricted to a μm-scale gap between the plates of the SlipChip (“dead-end flow”). Rupture of the lubricating oil layer (reminiscent of a Cassie-Wenzel transition) was proposed as a cause of discrepancy between the model and the experiment. Both dilute salt solutions and complex biological solutions such as human blood plasma could be flowed using this approach. We anticipate that flow driven by capillary pressure will be useful for design and operation of flow in microfluidic applications that do not require external power, valves, or pumps, including on SlipChip and other droplet- or plug-based microfluidic devices. In addition, this approach may be used as a sensitive method of evaluating interfacial tension, contact angles and wetting phenomena on chip.

Correspondence to: Rustem F. Ismagilov.

rustem.admin@caltech.edu .

Supporting Information Available. Movies, experimental details, and additional figures, tables, and equations. This information is available free of charge via the Internet at http://pubs.acs.org.

Disclosure: R.F.I. has a financial interest in SlipChip LLC.

INTRODUCTION

In this paper we present a strategy and describe conditions necessary for spontaneous flow of non-wetting droplets driven by capillary forces through confining microfluidic channels (Figure 1). Fluid flow is critical to most applications of microfluidic devices, including point-of-care assays such as glucose monitors that must transport an aqueous sample from a loading region to an assay region. As a result, much effort has gone into developing robust methods of controlling flow on microfluidic chips.[1-3] In a laboratory setting, the most common means of driving flow is a commercially-available electrically powered pump, but these pumps can be bulky or expensive. Other means include electrowetting for sessile droplets[4] and active control of on-chip valves.[5] These methods provide excellent control over initiating and stopping flow, rate of flow, and reconfiguring flow, but require an electric power supply and/or external pressure controls. For applications of microdevices in settings with limited resources or minimally trained users, passive or spontaneous means of driving flow are preferable. In particular, there is a need for approaches for controlled power-free flow in liquid-liquid droplet systems, which provide many advantages for chemical and biological assays.[6-11]

While several methods of generating power-free or spontaneous fluid flow are available, none can provide on-demand initiation and direction of spontaneous flow of droplets with controllable flow rate. Simple methods such as wicking[12-15] are better suited to flow of single phases than to flow of intact microdroplets, while gravity[16-18] is best for slow, unidirectional flow. Pressurized flow has been initiated with on-chip gas generation[19] or aspiration into pre-evacuated devices,[20-22] though repeated starting and stopping was not possible and the latter required precise timing between the pre-evacuation and the use of the device. Spontaneous flow of droplets on the microscale is more readily controlled via capillary pressure, which depends on interfacial tension, wettability (contact angles), and geometry.[23-27] Several strategies for passive or predefined control of liquid-liquid droplet motion based on capillary pressure have been developed, including utilization of gradients of surface tension,[28] patterns of wettability,[29-31] or geometric constraints.[32-35] For example, capillary hysteresis was shown to drive the flow of water droplets into a bird's moving beak as it drinks.[36] Capillary pressure of a bubble or droplet at a narrow junction was used to produce a valve[37] or shift register;[34] initiation of flow was controlled by modulating external fluid pressure. The additional challenge we are addressing here is to control the initiation, direction, and rate of spontaneous flow of droplets.

To address the need to start or reconfigure flow after a delay from when the sample is loaded, while having the simplicity of passively pre-programmed flow rates, we used the recently-developed SlipChip platform. The SlipChip was designed to manipulate fluid and droplet motion in a straightforward manner[38] and was used for applications ranging from protein crystallization[39,40] and immunoassays[41] to multiplexed,[42] digital,[43,44] and isothermal nucleic acid analysis.[45] A SlipChip can be assembled from two pieces of patterned glass or plastic with a layer of oil sandwiched in between. The two pieces are not bonded and can move easily relative to one another. Fluid manipulations are controlled by simply slipping the plates relative to one another (Fig. 1B,C), creating and reconfiguring fluid paths.[38,46]

In this paper, we present a means of controlling the spontaneous flow of droplets by using geometric constraints on capillary pressure in a reconfigurable SlipChip device (Fig. 1D). This method of inducing flow is distinct from flow induced by continuously moving plates relative to each other, as in shear-driven chromatography.[47,48] We developed and tested a physical model of the pressures that control the flow, and developed strategies to understand and control critical parameters such as contact angle hysteresis and lubrication by the oil

layer. The model successfully predicted initiation and rates of flow through microfluidic channels, including flow rates for two complementary mechanisms of liquid transport. Finally, we tested the flow of biological solutions that would ultimately be used in diagnostic applications.

RESULTS AND DISCUSSION

Physical model of flow of droplets driven by capillary forces in microfluidic channels

A simple physical model was developed to describe the flow of non-wetting droplets through channels, based on the balance of capillary pressure and pressure due to flow resistance.

Capillary pressure drives flow—We used capillary pressures to control initiation and rate of spontaneous flow (Figure 1). Qualitatively, a nonwetting droplet ($\theta > 90°$; Fig. 1A) is driven forward by capillary pressure if there is greater curvature at the back of the droplet than at its front.[32] This process differs from wicking, in which a wetting droplet ($\theta < 90°$) is pulled forward by capillary pressure towards greater curvature, often through a porous medium. The capillary pressure, ΔP_{cap} [Pa], at the liquid-liquid interface between a non-wetting aqueous droplet and an immiscible wetting oil is determined by the liquid-liquid interfacial tension, γ [N/m], the three-phase contact angle, θ [rad] (Fig. 1A), and the geometry of the device, and for a rectangular channel of width w_i [m] and height h_i [m] it is described by[49]

$$\Delta P_{cap\ \ i} = \gamma \cos\theta \left(\frac{2\,(w_i + h_i)}{w_i h_i} \right) = 2\gamma \cos\theta \left(\frac{1}{w_i} + \frac{1}{h_i} \right) \quad (1)$$

The capillary pressure at the front of the droplet, $\Delta P_{cap\ 2}$, opposes the pressure from the back of the droplet, $\Delta P_{cap\ 1}$ (Fig. 1D). Spontaneous flow occurs if and only if the net capillary pressure $\Delta P_{cap\ 1} - \Delta P_{cap\ 2}$ is positive, and the driving force is stronger for liquid pairs that have higher interfacial tension. In this paper, positive capillary pressures were obtained by slipping small capillaries into contact with larger channels (Fig. 1 B,C) to initiate flow.

Contact angle hysteresis reduces driving pressure—The surface chemistry of the substrate plays a significant role in controlling capillary-driven flow on-chip, entering into the predictions via the contact angle θ. In preliminary tests, we observed that flow rate varied significantly with surface chemistry even when geometry was kept constant— flow was slow (μm/s) on fluorosilanized glass and rapid (mm/s) on FEP-dipcoated glass (data not shown). Stationary contact angles on these surfaces (θ_S >145° and θ_S ~ 160°, respectively) could not account for these differences in flow rate, so we tested whether contact angle hysteresis[50,51] could. Contact angle hysteresis, or the difference between advancing and receding contact angles, θ_A and θ_R respectively, was measured on each surface by measuring θ as volume was added to and then removed from an aqueous droplet (0.1 M $Fe(SCN)_3$)[52] under oil (see supporting Materials and Methods and SI Fig. 1). We found that the surface-treatment protocols used for fluorosilanization and FEP-dipcoating produced high (θ_A- θ_R, ~ 45°) and low (≤ 5°) hysteresis, respectively, under FC40 oil (SI Table 1 and SI Fig. 2). To include contact angle hysteresis in the model, the pressure at the front of the droplet ($P_{cap\ 2}$) was defined using θ_A, and the pressure at the back of the droplet ($\Delta P_{cap\ 1}$) was defined using θ_R (Fig. 1D):

$$\Delta P_{cap\ \ 2} = 2\gamma \cos\theta_A \left(\frac{1}{w_2} + \frac{1}{h_2}\right) \tag{2a}$$

$$\Delta P_{cap\ \ 1} = 2\gamma \cos\theta_R \left(\frac{1}{w_1} + \frac{1}{h_1}\right) \tag{2b}$$

In this model, higher contact angle hysteresis lowers the driving force for flow. Consistent with the preliminary observations, the model predicts that on a surface with high contact angle hysteresis, capillary-driven flow is slow or even stops. This description of capillary pressure assumes that the front of the droplet moves forward. Therefore, a negative value of $\Delta P_{cap\ 1}$ - $\Delta P_{cap\ 2}$, obtained in systems with very high hysteresis, predicts only that no flow occurs and should not be taken to imply backwards flow.

Viscous resistance balances the pressure—While capillary pressure alone provides the driving force for spontaneous flow, the flow rate is set by the balance of capillary pressure with viscous flow resistance. To calculate flow resistance on-chip, we approximated the geometry of an isotropically etched channel as a rectangle with width equal to the maximal width of the etched channel. In general, the flow resistance P_{drag} / Q [N] of a fluid with viscosity μ_i [Pa·s], moving with volumetric flow rate Q [m^3/s] through a rectangular channel that has $h_i < w_i$ and length L_i [m], can be described by[23]

$$P_{drag} / Q = \frac{\pi^4 \mu_i L_i}{8 h_i^3 w_i \left(1 - \frac{2h_i}{\pi w_i} \tanh\left(\frac{\pi w_i}{2h_i}\right)\right)} \tag{3}$$

With a cubic dependence on h_i, flow resistance rapidly becomes large as h_i decreases. The total resistance through a fluid path through multiple channels is found by adding the individual resistances of each channel, either in series (e.g. a + b + c, where a, b, and c are individual flow resistances) or in parallel (e.g. 1/(1/a + 1/b + 1/c)) as appropriate.

The flow rate Q through each path on the chip was calculated by equating the net capillary pressure ($\Delta P_{cap\ 1}$ - $\Delta P_{cap\ 2}$, from Eq. 2) with the total pressure due to flow resistance (from Eq. 3). For example, for channels i that are connected in series, the flow rate is given by

$$Q = \frac{\Delta Pcap1 - \Delta Pcap2}{\sum_i \frac{\pi^4 \mu_i L_i}{8 h_i^3 w_i \left(1 - \frac{2h_i}{\pi w_i} \tanh\left(\frac{\pi w_i}{2h_i}\right)\right)}} \tag{4}$$

Using the model of capillary pressure versus flow resistance, we derived and tested predictions for the initiation of flow (set by capillary pressure alone) and the rate of flow (set by the ratio of capillary pressure and flow resistance).

Initiation and routing of flow into an oil-filled channel is controlled by overlap

For flow on chip to be most useful, it should initiate immediately after the fluidic pathways are connected and not before. This property would allow for loading and storing a sample solution on-chip and then later starting an assay by slipping the chip to initiate flow. We derived a requirement for initiation of flow and tested it on chip. The requirement for

positive net capillary pressure was used to predict the minimum overlap distance between the capillary and the oil-filled channel that would permit initiation of spontaneous flow (Figure 2A). Immediately after slipping, $\Delta P_{cap\ 2}$ is calculated at the junction between the capillary and the channel and is set by the width of the capillary w_1 and the length of the overlap between the capillary and the channel, x. Since flow should initiate only when $\Delta P_{cap\ 1} > \Delta P_{cap\ 2}$, by using Eq. (2) and rearranging we obtained the geometric requirement that

$$\left(\frac{1}{w_1}+\frac{1}{h_1}\right)>\frac{\cos\theta_A}{\cos\theta_R}\left(\frac{1}{w_1}+\frac{1}{x}\right) \tag{5}$$

This requirement set a minimum value of the overlap x that was required to initiate flow. In systems that have negligible contact angle hysteresis, this requirement simplified to

$$x>h_1 \tag{6}$$

Using similar arguments, the model predicted that once the flow has initiated and filled the cross-section of the receiving channel, it will continue as long as the channel is larger than the capillary (see supporting results in SI, p. S8). Thus, initiation is the only barrier of interest.

We tested whether Equation (5) correctly described the threshold amount of overlap x between the capillary and channel that was required for flow to initiate (Figure 2a). We designed a set of simple SlipChips with four pairs of capillaries and channels that had varying values of x (Figure 2b), from 10 to 150 μm, in duplicate. Capillaries were located on the bottom plate of the chip (h_1 = 32, 50, or 65 μm), with channels on the top plate (h_2 = 85 μm). Chips were assembled with FC40 oil, an aqueous solution (0.1 M $Fe(SCN)_3$) was loaded into the capillaries, and the chip was slipped laterally to connect the capillaries with the receiving channels (SI Fig. 3). Controlled slipping in the lateral direction was accomplished using an XY- micromanipulator to move the top plate relative to the bottom plate with better than 10 μm precision (see Materials and Methods in SI, and SI Fig. 4). After each experiment, the occurrence of flow and the overlap distance x were measured for each capillary using an image taken on a stereomicroscope (Fig. 2b *insets*). We used a surface with high contact angle hysteresis (fluorosilanized glass), to reduce the driving force for flow so that manual control of the overlap could provide sufficient resolution, and to prevent break-up of droplets due to capillary instabilities through a large expansion in depth (see below).

From these experiments we found that flow initiated only when ($1/w_1 + 1/h_1$) exceeded ($1/w_1 + 1/x$) (Figure 2d), in agreement with predictions. Flow occurred when the overlap was greater than 1.75-fold the depth of the capillary, $x > 1.75h_1$ (Figure 2c). The model predicts that for surfaces with lower contact angle hysteresis, the scaling factor (1.75) will decrease to 1 (Eq. 6), but this remains to be tested in future work.

Control of overlap also provided a means to control the direction, or routing, of flow (Figure 3). After filling the capillaries, they could be slipped to overlap with different channels. The direction of flow could be controlled even when the capillary overlapped with both channels simultaneously (Figure 3c*i*), as a function of which channel had the greater overlap distance. Routing could also be controlled by choosing which channel contacted the capillary first or at all (Figure 3c*ii*).

Predictions for two regimes of flow rate based on flow resistance

To predict the flow rate of spontaneous flow driven by capillary pressure, we considered the dominant terms for flow resistance in various geometries of the chip. In our experiments on the SlipChip, as the droplet flows out of the capillary, the free volume has to be replaced by oil flowing into the capillary. As the droplet enters the receiving channel, it has to displace the oil already in the channel. Therefore, in addition to flow resistance provided by the droplet itself, the flow resistance of the oil leaving the receiving channel and entering the capillary must be considered. Oil can flow either through the gap between the plates (h ~ 1 - 10 μm) or through a channel provided for that purpose (h ~ 10 – 150 μm). The cubic dependence of flow resistance on height (Eq. 3) led to predictions for two regimes of flow (Figure 4), differing dramatically in the magnitude of the flow rate. Chips were designed to test the predictions in each regime of flow.

Flow regime (I): Oil flows through connections to reservoirs—In this regime (Figure 4a), the ends of the capillaries and channels are connected to “oil reservoirs” that are open to the air and provide entry and escape paths with negligible resistance to flow. Holes were drilled through the top plate of the SlipChip to provide access to the air, and oil was located only inside the chip or bathed its top surface in a uniform layer; the reservoirs therefore did not contribute to the driving pressure for flow. In this situation, the resistance to flow of the droplet is given by the sum of three resistances in series – that of the oil inlet channel, the capillary, and the receiving channel:

$$\sum\left(P_{drag}/Q\right)=\frac{\pi^4\mu_{oil}L_0}{8h_0^3w_o\left(1-\frac{2h_0}{\pi w_0}\tanh\left(\frac{\pi w_0}{2h_0}\right)\right)}+\frac{\pi^4\left(\mu_{aq}+\mu_{oil}\right)(L_1/2)}{8h_1^3w_1\left(1-\frac{2h_1}{\pi w_1}\tanh\left(\frac{\pi w_1}{2h_1}\right)\right)}+\frac{\pi^4\left(\mu_{aq}+\mu_{oil}\right)(L_2/2)}{8h_2^3w_2\left(1-\frac{2h_2}{\pi w_2}\tanh\left(\frac{\pi w_2}{2h_2}\right)\right)} \quad (7)$$

Note that because of the differing cross-sectional areas ($w_i \cdot h_i$) of each channel, the resistances must be summed in terms of pressures (as shown here) instead of in terms of forces. We approximated the time-dependent resistance terms in the capillary and receiving channel with the resistance when each is filled with half aqueous and half oil. To approximate the resistance to the flowing droplet, we used Eq. 3, which describes single-phase flow, thereby neglecting the contribution of internal fluid recirculation. The total resistance thus obtained (Eq. 7) was used in conjunction with the net capillary pressure to predict the volumetric flow rate Q (Eq. 4). Q is independent of x (for large x, see Conclusions) and the dimensions of the gap between the plates.

For the geometries tested here, this model predicted flow rates as fast as 10 - 100 nL/s (i.e. 1-10 mm/s) over a wide range of conditions, e.g. for aqueous droplets with low hysteresis (< 10 deg), moderate or high surface tension (10 – 80 mN/m), and low viscosities (aq ~ 1 mPa·s, oil < 10 mPa·s). Slower flow could be obtained in the same geometries by increasing the viscosity, lowering the surface tension, or raising the hysteresis. Rapid flow rates such as these may be useful for washing or for transfer of solutions between modular assay components on a diagnostic chip.

Flow regime (II): Oil flows through gap—If open reservoirs are omitted or detached from the capillary and/or the channel on SlipChip, then the flow of lubricating fluid must

pass through the gap or along the sides of the aqueous droplet (Figure 4b), with up to 1000-fold greater flow resistance as a result. The resistance to flow through the μm-high gap between the plates of the SlipChip is described as follows[46]:

$$\sum P_{drag\quad gap} / Q = \frac{\pi^4 \mu_{oil} L_3}{8 {h_3}^3 w_3} \tag{8 a}$$

where h_3, w_3, and L_3 are the height, width, and length of the oil path through the gap. For simplicity, we approximated L_3 as the straight-line distance from the front to the back of the droplet. This is a minimal estimate; a curved path, as shown in Fig. 4b (grey arrows), would be longer and have higher resistance. In addition to flowing through the gap, oil can also flow within the capillary, in the space between the capillary wall and the aqueous droplet:

$$\sum P_{drag\quad capillary} / Q = \frac{\pi^4 \mu_{oil} L_3}{16 h_4^3 w_4 \left(1 - \frac{2h_4}{\pi w_4} \tanh\left(\frac{\pi w_4}{2h_4}\right)\right)} \tag{8 b}$$

where h_4 and w_4 are the height and width of the oil path (see supporting Materials and Methods on how these dimensions were calculated), defined such that $h_4 < w_4$. Recalling Equation 3, we select the smaller dimension to be h_4 because it contributes the most to the resistance. In the glass-etched channels we used, there are two parallel paths for oil, one on each side of the droplet ("side paths"), so an extra factor of ½ was included in Eq. 8b. The total resistance was described as the sum of these two resistances in parallel:

$$\sum \left(P_{drag} / Q\right) = \frac{\pi^4 \mu_{oil} L_3}{8 {h_3}^3 w_3 + 16 h_4^3 w_4 \left(1 - \frac{2h_4}{\pi w_4} \tanh\left(\frac{\pi w_4}{2h_4}\right)\right)} \tag{8 c}$$

This equation was used to obtain the flow rate Q (Eq. 4). The path of the oil must be predicted for each chip design based on the path of least resistance, where resistance is estimated using Eq. 8. For example, if open oil reservoirs are located close to the capillary and channel (small L_3), then oil should flow linearly between them. If reservoirs are distant or absent, then oil should flow in a recirculating loop as it is displaced from the receiving channel, flows backwards through the gap and alongside the droplet, and finally enters the capillary (Figure 4b). In either case, when $h_3 > 3$ μm, Q was predicted to scale with $1/{h_3}^3$ in this flow regime. When $h_3 < 3$ μm, the path of least resistance is always through the sidepath in the capillary, and thus further reductions in gap height were not predicted to significantly affect the flow rate.

For the geometries tested in this paper, Eq. 8 predicted flow rates as slow as ~ 800 pL/s (i.e. ~ 0.8 μm/s) for small (<3 μm) gap heights, which may be useful for perfusion cultures or slow and steady wash steps. Increasing the gap size to 8 μm increased the prediction to up to ~30 μm/s for viscous oil (55 mPa s), and more than 500 μm/s for low viscosity oil (3 mPa s). Thus, the model predicted that manipulation of gap height and the carrier phase could produce a range of flow rates in the gap-limited flow regime; this versatility could be useful in providing faster flow in situations where introducing a reservoir would be inconvenient.

Experimental control of rate of flow when oil moved through channels

In flow regime I, three resistance terms contributed to the predicted flow rate: flow of oil from a reservoir through an inlet channel, flow of aqueous and oil through a small capillary, and flow of aqueous and oil through a receiving channel to another reservoir (Eq. 7). For the

geometries and viscosities used here, all three terms were of magnitude $10^{11} – 10^{12}$ Pa s/m^3, with the term for the shallow capillary usually 2 – 10 -fold larger than the other terms. Thus, the dimensions of the capillary were predicted to have the largest effect on flow rate, but all three components of the flow path had to be taken into account.

We designed chips to test whether Q varied as predicted with the length, width, and depth of the capillaries and channels (Figure 5a,b, SI movie 1). As before, capillaries in the bottom plate were shallower than the channels in the top plate ($h_1 < h_2$), to provide the driving force for flow. Four pairs of capillaries and channels with varying widths and lengths were included on each chip, in duplicate (SI Fig. 5), and three chip depths were tested. Capillaries and receiving channels were slanted so that a single horizontal slip connected the capillary to both the oil inlet channel and the receiving channel simultaneously, to initiate flow. We used a dichlorodimethylsilanized glass surface and a strongly wetting oil (polydimethylsiloxane (PDMS oil), 57 cSt, i.e. 55 mPa·s) with 0.01 mg/mL Span80, to minimize contact angle hysteresis (SI Table 1 and SI Fig. 2) and protect the aqueous droplets from adhesion to possible defects in the surface.

In preliminary experiments on chips with low contact angle hysteresis, stretching or breakup of the flowing droplets occurred at or near the junction between the capillary and the channel. We hypothesized that stretching and breakup were due to capillary instability of the droplets as they passed through the sudden expansion into the channel. Consistent with this hypothesis, breakup was reduced or avoided by reducing the height differential between the capillary and the channel (demonstrated in experiments below), reducing the suddenness of the expansion with a flared shape (SI Fig. 6), reducing the driving force by adding surfactants to the aqueous and/or oil phase (data not shown) or using a surface with higher hysteresis (demonstrated in Initiation section). Chips used to further test predictions of flow rate were designed with a small vertical expansion (< 15% increase from h_1 to h_2) and a flared shape.

We generated predicted flow rates (μm/s) for each condition on each chip (Eq. 4 with Eq. 7), based on geometry (measured by a profilometer), aqueous-oil interfacial tension and advancing/receding contact angles and hysteresis on the surface (measured by a goniometer for each batch of silanization), and the viscosity of the oil phase (SI Table 1). The viscosity of the aqueous phase (0.1 M $Fe(SCN)_3$) was set to 1 mPa·s.[52] There were no free or adjustable parameters in the model; everything was measured experimentally.

Finally, we measured flow rates on each chip and plotted observed versus predicted flow rates for all depths, widths, and lengths of capillaries and channels tested (Fig. 5C and SI Table 2). The flow rates scaled in agreement with the model, with < 12% deviation from the predictions over a range from 100 to > 500 μm/s. Droplets in the 53 μm and 68 μm-deep capillaries moved smoothly, without a change in shape of the ends of the droplets. With this viscous oil (55 mPa s), the flow slowed down slightly over time, by ~ 20 – 40% of its initial rate, and slowing was most pronounced in the longer capillaries. This degree of slowing was predicted by the physical model, as the more-viscous oil replaces the less-viscous aqueous phase in the capillary and raises the overall resistance in this part of the fluid path.

In the shallowest capillaries (36 μm), the initial flow rate deviated by up to 35% from the model predictions over a range from 30 to 130 μm/s, and the slowing (by 50 – 70%) exceeded the model's predictions. The back end of the droplets in these shallow capillaries was observed to drag slightly along the surface occasionally, as though catching on small defects in the surface, especially with the slowest droplets.

Robustness of the flow to varying oil viscosity and surface energy

We next tested how robust the system was to varying oil viscosity and surface energy. We hypothesized that the dragging and slowing observed in the shallowest channels with viscous oil (55 mPa·s) were a consequence of thinning and rupture of the oil layer that normally protects aqueous droplets from the surface.[52,53] We observed accumulation of oil droplets underneath the aqueous droplets (Figure 6A and SI Fig. 7) and interpreted this phenomenon as rupture of the oil layer. We predicted that rupture would increase the interaction between the droplet and the surface and increase the contact angle hysteresis compared to what can be measured on the goniometer, where the oil layer remains intact.

To test the prediction that an intact oil layer was required for flow to follow the predictions of the model, we repeated the experiments of the previous section using an oil of lower viscosity (3.1 cSt, i.e. 2.76 mPa s), again including 0.01 mg/mL Span80 in the oil solution. Lower oil viscosity should accelerate the drainage of oil from under the droplet and facilitate rupture[54]; this is a kinetic effect. Flow through this oil was rapid, up to 8 mm/s (6 μL/min, see Figure 6B and SI Table 3), but deviation from the model increased slightly; on average the flow rates were 2-fold slower than predicted. Consistent with rupture of the oil layer, droplets of oil were visibly trapped underneath several aqueous droplets, and aqueous droplets sometimes dragged slightly at their receding edge, especially in the shallowest capillaries.

Besides lowering the viscosity, we also predicted that oil rupture would be more likely if the surface energy of the oil was increased; this is a thermodynamic effect. In air, a fluid can completely wet a surface only if the fluid has a surface energy, γ, (surface tension, mN/m, measured in air) that is lower than the critical energy of the surface.[49] The surface tension of many silicone fluids is 19 – 22 mN/m, while the surface tension of liquid alkanes is usually higher, 23- 28 mN/m. The critical surface energy of alkyl-silanized glass with typical partial molecular coverage is 24-28 mN/m, so in general, silicone oils wet better than alkanes on a methyl-silanized surface.[49]

Tetradecane without surfactant is commonly used on hydrophobic chips,[43,55,56] and we tested the robustness of flow of aqueous droplets in this oil. We predicted that an oil layer of tetradecane (γ ~ 27-32 mN/m) was more likely to rupture than a layer of 3 cSt PDMS (γ ~ 19.2 mN/m, manufacturer specifications). First we compared the contact angles and hysteresis of aqueous (0.1 M $Fe(SCN)_3$) droplets in each oil on the same methyl-silanized glass surface. Consistent with its higher surface energy, using tetradecane decreased the contact angles and raised the hysteresis of aqueous droplets (θ_A ~ 172, θ_R ~ 171 in 3cSt PDMS; θ_A ~ 149-152, θ_R ~ 140-145 in tetradecane). Next, we measured the flow rates of aqueous droplets in tetradecane, using the same chip geometries as for experiments with PDMS oils (Fig. 5A,B). Using tetradecane as the oil phase resulted in larger deviations from the model (5 to 10-fold slower than predicted, Figure 6C and SI Table 4). In some cases, the flow rate in tetradecane reduced suddenly from mm/s to μm/s, varying across a single chip or over time in a single channel, consistent with a sudden rupture of the oil layer. Using a more viscous hydrocarbon (mineral oil) did not restore the speed or stability of flow.

From the experiments in this section and the previous section we concluded that the model of capillary pressure and viscous resistance had excellent agreement with experimental systems when the protective oil layer remained intact around the aqueous droplet. If the oil layer appeared to rupture because of high pressure caused by tight curvature of the aqueous droplet in shallow channels, a low oil viscosity, or poor wetting by the oil, then the droplets flowed slower than predicted because of increased drag on the surface.

Control of rate of flow when oil moved through the gap between the plates

In flow regime II, there are no channels for transport of oil to or from a reservoir, and it must travel through the μm-high gap and the side paths. The predicted flow resistance of this combined path (Eq. 8), ~ 10^{15} - 10^{16} Pa s/m^3, is over 1000-fold greater than the predicted resistance in the capillaries and should dominate the dynamics of flow. We designed a chip to test the predictions of this model (Figure 7a and SI Movie 2). As before, capillaries in the bottom plate were brought into contact with channels in the top chip by a single slip (SI Fig. 8). The width and lengths of the capillaries and channels were varied, while depths were kept constant (80 and 85 μm, respectively). Each capillary and its receiving channel were isolated together on-chip by using aqueous barriers to prevent oil flow from the edges of the chip or from adjacent capillaries. With these barriers, oil must flow in a recirculating path from the channel back to the capillary (illustrated in Fig. 4B).

Each parameter of the model for flow of oil in this regime (Eq. 8c) was specified in the context of this chip design. To achieve the required precision of gap height, we added glass-etched microposts[40] to the top of the chip (see SI) and developed methods to robustly measure the height of gap[46] before each flow trial (see SI). We found that the gap height was 2.8 – 4.4 μm and 5.6 – 6.8 μm on chips with 2- and 5-μm microposts, respectively, and we used these values to generate predictions of flow rate (Eq. 4 with Eq. 8c) for each trial. The width of the path through the gap, w_3 (sketched in Fig. 4b), was approximated as the distance between the aqueous barriers flanking each capillary (here, 2770 μm). The length of the path, L_3, was set to the average of the final and initial length of the droplet (see SI for equation and SI Table 7 for calculated values). The side-path for oil is irregularly shaped (Fig. 7b) and was approximated as a rectangle to permit calculation of flow resistance of oil within it (see SI methods). As before, there were no free or adjustable parameters in the model.

Finally, we tested the predictions of the model by measuring the flow rate in each channel at various gap heights, using 55 mPa·s PDMS oil. The observed flow rates ranged from < 1 to 20 μm/s and scaled as expected with gap height, length, and the widths of the capillaries and channels (Fig. 7C and SI Table 5). Accumulated droplets of oil were observed under the aqueous phase (SI Fig.7), suggesting that the oil layer was ruptured, possibly because of the long path length and high pressure that was required for filling. Consistent with this observation, most observed flow rates were slower (less than 3-fold difference) than the predicted flow rates. In a single trial the observed flow rates exceeded the predicted flow rates; this trial was performed on a chip with 2 μm microposts and a measured gap height of 4.4 μm. When lower viscosity oil was used (3 mPa·s), the flow rates increased up to ~ 200 μm/s and again followed the general trends of the predictions (SI Fig. 9). However, the data were noisier and deviations increased (up to 6-fold slower than the predictions). We hypothesize that with a large gap height or less viscous oil, the height of the gap could transiently fluctuate in response to the motion of aqueous droplets and alter the rate of flow, but this hypothesis remains to be tested. In summary, these experiments showed that the model for flow of oil through a μm-scale gap of known height provided a good approximation of the experimental system.

Flowing complex solutions

We tested whether capillary pressure could predictably induce spontaneous flow of complex solutions of interest to biomedical diagnostics or basic science. Such solutions often contain surfactants, proteins, or other surface active molecules, which can be susceptible to adsorption on surfaces during flow. Adsorption on surface results in increased surface-aqueous interactions (“sticking”), an increase in contact angle hysteresis and a corresponding decrease in flow rate. Adsorption has been prevented previously by using oil-

soluble surfactants with oligoethylene glycol headgroups.[57,58] The model can accommodate the effects of sticking and/or surfactants by using experimentally measured hysteresis values for each biological sample in the oil solution of interest. As a first qualitative investigation, we tested whether spontaneous flow of complex ("sticky") solutions was possible in the presence or absence of protective surfactants.

We observed that such "sticky" solutions did not flow spontaneously when the oil layer appeared to be ruptured. On methyl-silanized chips, droplets containing 1 mg/mL BSA always caused rupture of the oil layer, even with 55 mPa·s silicone oil as the carrier fluid and regardless of what surfactants were used in the oil. Polyethylene glycol sorbitan monooleate (Tween-80, Sigma-Aldrich), PEG-terminated siloxane (SIH-6185.0, Gelest), and PEG-linked silicone (CMS-222, Gelest) all failed to protect the aqueous droplet, and the BSA solution did not flow spontaneously in any of these experiments. We speculated that an intact oil layer is required to prevent adsorption of proteins or other molecules to the surface.

To achieve robust wetting of the solid surface by the oil in the presence of aqueous surfactants, we used a Teflon-like surface with a lower critical surface energy (15 ± 2 mN/m).[49] Clean glass chips were coated with a micron-scale layer of FEP by dip-coating (see SI). This surface coating is rough on the μm scale, and in preliminary experiments we found that it produced gap heights on the SlipChip of ~ 6-10 μm. We used the chips from flow regime I (Fig. 5A,B) so that the height of the gap would not affect the flow rate significantly. FC40, a fluorinated oil, was used as the carrier fluid for flow experiments. First we tested whether spontaneous flow occurred with no surfactant added to the oil. Without surfactant, a 1 mg/mL BSA solution did not flow spontaneously and the FEP-coated surface was made permanently hydrophilic by contact with the BSA. Next, we tested flow using FC40 with 1 mg/mL RfOEG ($CF_3(CF_2)_7CH_2(OCH_2CH_2)_3OH$), a fluorous surfactant with a tri-ethylene glycol headgroup.[57,59] This concentration of RfOEG was previously used to prevent droplets of clotted and unclotted human plasma from adhering to a Teflon-coated PDMS channel.[60] In addition to 1 mg/mL BSA solution, we also tested spontaneous flow of a serum-free cell culture medium (AIM-V, Gibco) and fresh whole human blood (citrated). These solutions were loaded carefully onto the chip to avoid pushing them into the gap, and flowing was initiated by slipping. Each of these "sticky" solutions flowed smoothly, without apparent dragging or slowing, at flow rates on the order of 100 μm/s (Figure 8 and SI Movie 3). These flow rates were similar to the flow rate of phosphate-buffered saline in the same oil solution, which suggested that RfOEG may have saturated the oil-water interface and therefore blocked exposure of the aqueous surfactants.

In summary, "sticky" solutions flowed spontaneously as long as the oil layer remains intact around the droplet and leakage into the gap was avoided. This feature should make this method of controlling spontaneous flow broadly useful for future applications. As mentioned above, the SlipChip platform has been validated for sample handling and multi-step assays in several biological contexts, including protein crystallization[39,40], immunoassays for detection of insulin[41], multiplexed[42] and digital PCR,[43,44] and isothermal nucleic acid analysis.[45] Combining the spontaneous flow demonstrated here with such assays could enable new developments towards clinical diagnostics or laboratory microassays.

CONCLUSIONS

This paper showed that spontaneous flow of non-wetting aqueous droplets can be driven by capillary pressure, and that its initiation and flow rate can be precisely controlled by geometric constraints on the SlipChip. A simple physical model of capillary pressure and viscous flow resistance was sufficient to describe the rate of flow in systems where the oil

lubricating layer around the aqueous droplet remained intact. We proposed that rupture of the oil layer led to slower flow and adsorption of aqueous surfactants, and conditions that promote rupture of the oil layer were identified and tested. The observed flow rates controllably spanned 4 orders of magnitude, from < 1 μm/s to ~ 8 mm/s (~ 50 nL/min to 6 μL/min). With an intact oil layer, even "sticky" aqueous solutions such as whole human blood flowed spontaneously and smoothly.

Though the physical model was sufficient to describe the flows observed here to within 3-fold in 55 mPa·s oil, there are several additional factors that could be included to better describe future applications of capillary-pressure driven flow. Flow resistance for droplets was modeled as though for a single phase flowing through a rectangular cross-section, and could be improved to account for additional resistance from internal recirculation and to reflect the rounded cross-section of the droplet. The side path for the backwards flow of oil in regime II was also modeled as a rectangular cross-section of a fixed size; future models and experiments could address its irregular shape and test whether it varies with gap height, filling pressure, capillary geometry, and contact angle. For flow through narrow overlaps, it may be useful to include the resistance at the overlap between the capillary and the channel; preliminary calculations (based on the length of the overlap x as the height of the neck, the total height $h_1 + h_2$ as the length of the neck, and w_2 as the width of the neck) indicated that an overlap greater than 50 - 80 μm in length produced a resistance that was negligible compared to that of the capillary or the channel. Additionally, the model described here defined the capillary pressure at the front of the droplet by using the curvature of the droplet after it completely filled the width of the channel. Capillary pressure for a droplet that is expanding freely from the end of a capillary tube has been modeled recently,[32] and this model could be adapted in the future to describe a droplet expanding in two dimensions within a receiving channel.

Marangoni effects, which can arise from motion of surfactants at the droplet-oil interface, were not included in our model. Forward motion of the droplet would be expected to sweep surfactants to the back of the droplet,[61] thus lowering the surface tension there and decreasing the driving force for flow.[62,63] Marangoni effects can affect microscale liquid/liquid systems[64] and have been quantified on-chip recently.[65] We did not observe such slowing with the low concentrations of oil-phase surfactants used in this work. However, preliminary experiments with higher concentrations of surfactants (e.g. 0.2 mg/mL Tween80 or 0.1 mg/mL hydroxy-terminated siloxane (Gelest SIH6185.0) in 55 mPa·s silicone oil) showed concentration-dependent slowing of the droplet over time and even complete cessation of flow in some cases. Thus, surfactants must be carefully selected to avoid Marangoni effects when capillary-pressure-driven flow is desired.

Contact angle hysteresis was probably much higher on-chip for a droplet with a ruptured oil layer than could be measured on the goniometer, which usually maintains oil layers intact. Rupture of the oil layer may be related to a Cassie-Wenzel transition from an unstable super-hydrophobic state to a slightly less hydrophobic state.[66] An interesting opportunity for future work would be to use this system to measure advancing and receding contact angles on-chip during flow,[67] on the top and bottom surfaces of a channel. This methodology would enable one to test whether the physical model is correct for systems with unstable oil layers if the actual contact angles were known, and would increase the applicability of the model.

We anticipate that this mechanism of control over droplet behavior will be useful wherever spontaneous, on-demand, or precisely directed or timed microscale flows are required.[1-3,5-11,68-73] Whereas flow driven by external pressure, e.g. with pumps, is dominated by the external force, spontaneous capillary-pressure driven flow is exquisitely

sensitive to interfacial phenomena, including the chemical composition of the two fluid phases and the surface, as well as the geometry of the fluids and channels. This level of control should be useful for design and operation of droplet-based microfluidic devices, including plug-based devices and SlipChip, and also may provide a sensitive method of evaluating interfacial tension or contact angles on chip. Because flow does not initiate until a slipping motion connects the capillary to the channel, different routes of flow could be chosen by changing the direction of slipping, for on-demand choice between different pre-programmed chip-based assays. Flow of biological solutions that suffer from surface adsorption will benefit from recent developments of methods to fabricate fluorinated chips[74-77] with a flat, smooth surface between the channels, so that the chip can have both a small gap and a low surface energy at the same time. Future work using this technology may include applications such as slow perfusion of on-chip cell cultures, separation of plasma from whole blood, or rapid delivery of sample solutions to multiple regions of a chip for parallel analyses.

Supplementary Material

Refer to Web version on PubMed Central for supplementary material.

Acknowledgments

This work was supported by DARPA Grant No. 11-39-DxOD-LRS-FP-016 and NIH Grant No. 1R01 EB012946 administered by the National Institute of Biomedical Imaging and Bioengineering. We thank Liang Li for discussions of chip design and oil rupture, Tom Witten for discussions of fluid instabilities, Stefano Begolo for discussions of pressures vs. forces, and for considering the Cassie-Wenzel transition and means to test it, and Toan Huynh for developing the FEP-dipping protocol. We thank Heidi Park for contributions to writing and editing this manuscript.

REFERENCES

1. Haeberle S, Zengerle R. Lab Chip. 2007; 7:1094. [PubMed: 17713606]
2. Luo Y, Qin JH, Lin BC. Frontiers in Bioscience. 2009; 14:3913. [PubMed: 19273322]
3. Squires TM, Quake SR. Reviews of Modern Physics. 2005; 77:977.
4. Fair RB. Microfluidics and Nanofluidics. 2007; 3:245.
5. Melin J, Quake SR. Annual Review of Biophysics and Biomolecular Structure. 2007; 36:213.
6. Song H, Chen DL, Ismagilov RF. Angew. Chem.-Int. Edit. 2006; 45:7336.
7. Pompano, RR.; Liu, W.; Du, W.; Ismagilov, RF. Annual Review of Analytical Chemistry. Vol. 4. Cooks, RGYES., editor. Vol. 4. 2011. p. 59
8. Kintses B, van Vliet LD, Devenish SRA, Hollfelder F. Curr. Opin. Chem. Biol. 2010; 14:548. [PubMed: 20869904]
9. Solvas XCI, deMello A. Chem. Commun. 2011; 47:1936.
10. Theberge AB, Courtois F, Schaerli Y, Fischlechner M, Abell C, Hollfelder F, Huck WTS. Angew. Chem.-Int. Edit. 2010; 49:5846.
11. Zagnoni, M.; Cooper, JM. Methods in Cell Biology, Vol 102: Recent Advances in Cytometry, Part A: Instrumentation, Methods. Vol. 102. Fifth Edition. Darzynkiewicz, Z.; Holden, E.; Orfao, A.; Telford, W.; Wlodkowic, D., editors. Elsevier Academic Press Inc; San Diego: 2011. p. 25
12. Martinez AW, Phillips ST, Carrilho E, Thomas SW, Sindi H, Whitesides GM. Analytical Chemistry. 2008; 80:3699. [PubMed: 18407617]
13. Martinez AW, Phillips ST, Whitesides GM. Proceedings of the National Academy of Sciences of the United States of America. 2008; 105:19606. [PubMed: 19064929]
14. Noh N, Phillips ST. Analytical Chemistry. 2010; 82:4181. [PubMed: 20411969]
15. Fu E, Lutz B, Kauffman P, Yager P. Lab Chip. 2010; 10:918. [PubMed: 20300678]
16. Du WB, Fang Q, He QH, Fang ZL. Analytical Chemistry. 2005; 77:1330. [PubMed: 15732915]

17. Millet LJ, Stewart ME, Sweedler JV, Nuzzo RG, Gillette MU. Lab Chip. 2007; 7:987. [PubMed: 17653340]
18. Yao B, Luo GA, Feng X, Wang W, Chen LX, Wang YM. Lab Chip. 2004; 4:603. [PubMed: 15570372]
19. Qin LD, Vermesh O, Shi QH, Heath JR. Lab Chip. 2009; 9:2016. [PubMed: 19568669]
20. Dimov IK, Basabe-Desmonts L, Garcia-Cordero JL, Ross BM, Ricco AJ, Lee LP. Lab Chip. 2011; 11:845. [PubMed: 21152509]
21. Hosokawa K, Sato K, Ichikawa N, Maeda M. Lab Chip. 2004; 4:181. [PubMed: 15159775]
22. Hosokawa K, Omata M, Sato K, Maeda M. Lab Chip. 2006; 6:236. [PubMed: 16450033]
23. Ichikawa N, Hosokawa K, Maeda R. Journal of Colloid and Interface Science. 2004; 280:155. [PubMed: 15476786]
24. Chan WK, Yang C. Journal of Micromechanics and Microengineering. 2005; 15:1722.
25. Bico J, Quere D. Journal of Fluid Mechanics. 2002; 467:101.
26. Walker GM, Beebe DJ. Lab Chip. 2002; 2:131. [PubMed: 15100822]
27. Lee SH, Heinz AJ, Shin S, Jung YG, Choi SE, Park W, Roe JH, Kwon S. Analytical Chemistry. 2010; 82:2900. [PubMed: 20210331]
28. Lagzi, I. n.; Soh, S.; Wesson, PJ.; Browne, KP.; Grzybowski, BA. J. Am. Chem. Soc. 2010; 132:1198. [PubMed: 20063877]
29. Chaudhury MK, Whitesides GM. Science. 1992; 256:1539. [PubMed: 17836321]
30. Daniel S, Chaudhury MK, Chen JC. Science. 2001; 291:633. [PubMed: 11158672]
31. Fang GP, Li W, Wang XF, Qiao GJ. Langmuir. 2008; 24:11651. [PubMed: 18788770]
32. Piroird K, Clanet C, Quéré D. Langmuir. 2011:9396. [PubMed: 21662237]
33. Metz T, Paust N, Zengerle R, Koltay P. Microfluidics and Nanofluidics. 2010; 9:341.
34. Zagnoni M, Cooper JM. Lab Chip. 2010; 10:3069. [PubMed: 20856984]
35. Abbyad P, Dangla R, Alexandrou A, Baroud CN. Lab Chip. 2011; 11:813. [PubMed: 21060946]
36. Prakash M, Quere D, Bush JWM. Science. 2008; 320:931. [PubMed: 18487193]
37. Peng XY. Lab Chip. 2011; 11:132. [PubMed: 20957289]
38. Du WB, Li L, Nichols KP, Ismagilov RF. Lab Chip. 2009; 9:2286. [PubMed: 19636458]
39. Li L, Du W, Ismagilov RF. J. Am. Chem. Soc. 2010; 132:106. [PubMed: 20000708]
40. Li L, Du W, Ismagilov RF. J. Am. Chem. Soc. 2010; 132:112. [PubMed: 20000709]
41. Liu W, Chen D, Du W, Nichols KP, Ismagilov RF. Analytical Chemistry. 2010; 82:3276. [PubMed: 20334360]
42. Shen F, Du W, Davydova EK, Karymov MA, Pandey J, Ismagilov RF. Analytical Chemistry. 2010; 82:4606. [PubMed: 20446698]
43. Shen F, Du W, Kreutz JE, Fok A, Ismagilov RF. Lab Chip. 2010; 10:2666. [PubMed: 20596567]
44. Kreutz JE, Munson T, Huynh T, Shen F, Du W, Ismagilov RF. Analytical Chemistry. 2011; 83:8158. [PubMed: 21981344]
45. Shen F, Sun B, Kreutz JE, Davydova EK, Du WB, Reddy PL, Joseph LJ, Ismagilov RF. J. Am. Chem. Soc. 2011; 133:17705. [PubMed: 21995644]
46. Li LA, Karymov MA, Nichols KP, Ismagilov RF. Langmuir. 2010; 26:12465. [PubMed: 20575548]
47. Desmet G, Baron GV. Analytical Chemistry. 2000; 72:2160. [PubMed: 10815980]
48. Cai Y, Janasek D, West J, Franzke J, Manz A. Lab Chip. 2008; 8:1784. [PubMed: 18941675]
49. de Gennes, PG.; Brochard-Wyart, F.; Quéré, D. Capillarity and Wetting phenomena: Drops, Bubbles, Pearls, Waves. Springer-Verlag; New York: 2004.
50. Gao LC, McCarthy TJ. Langmuir. 2009; 25:14105. [PubMed: 19627073]
51. Gao LC, McCarthy TJ. Langmuir. 2006; 22:6234. [PubMed: 16800680]
52. Tice JD, Song H, Lyon AD, Ismagilov RF. Langmuir. 2003; 19:9127.
53. Tice JD, Lyon AD, Ismagilov RF. Analytica Chimica Acta. 2004; 507:73. [PubMed: 17186061]
54. Persson BNJ, Mugele F. J. Phys.-Condes. Matter. 2004; 16:R295.

55. Shen F, Davydova EK, Du WB, Kreutz JE, Piepenburg O, Ismagilov RF. Analytical Chemistry. 2011; 83:3533. [PubMed: 21476587]
56. Shen F, Du WB, Davydova EK, Karymov MA, Pandey J, Ismagilov RF. Analytical Chemistry. 2010; 82:4606. [PubMed: 20446698]
57. Roach LS, Song H, Ismagilov RF. Analytical Chemistry. 2005; 77:785. [PubMed: 15679345]
58. Holtze C, Rowat AC, Agresti JJ, Hutchison JB, Angile FE, Schmitz CHJ, Koster S, Duan H, Humphry KJ, Scanga RA, Johnson JS, Pisignano D, Weitz DA. Lab Chip. 2008; 8:1632. [PubMed: 18813384]
59. Kreutz JE, Li L, Roach LS, Hatakeyama T, Ismagilov RF. J. Am. Chem. Soc. 2009; 131:6042. [PubMed: 19354215]
60. Pompano RR, Li HW, Ismagilov RF. Biophysical Journal. 2008; 95:1531. [PubMed: 18424502]
61. Scriven LE, Sternling CV. Nature. 1960; 187:186.
62. Barton KD, Subramanian RS. J. Colloid Interface Sci. 1989; 133:211.
63. Chen JN, Stebe KJ. J. Fluid Mech. 1997; 340:35.
64. Hanumanthu R, Stebe KJ. Physics of Fluids. 2007:19.
65. Martin JD, Marhefka JN, Migler KB, Hudson SD. Advanced Materials. 2011; 23:426. [PubMed: 20799293]
66. Moulinet S, Bartolo D. The European Physical Journal E: Soft Matter and Biological Physics. 2007; 24:251.
67. Zhu Y, Petkovic-Duran K. Microfluidics and Nanofluidics. 2010; 8:275.
68. Shui L, Eijkel JCT, van den Berg A. Advances in Colloid and Interface Science. 2007; 133:35. [PubMed: 17445759]
69. Clausell-Tormos J, Lieber D, Baret JC, El-Harrak A, Miller OJ, Frenz L, Blouwolff J, Humphry KJ, Koster S, Duan H, Holtze C, Weitz DA, Griffiths AD, Merten CA. Chem. Biol. 2008; 15:427. [PubMed: 18482695]
70. Frenz L, Blank K, Brouzes E, Griffiths AD. Lab Chip. 2009; 9:1344. [PubMed: 19417899]
71. Baret JC, Miller OJ, Taly V, Ryckelynck M, El-Harrak A, Frenz L, Rick C, Samuels ML, Hutchison JB, Agresti JJ, Link DR, Weitz DA, Griffiths AD. Lab Chip. 2009; 9:1850. [PubMed: 19532959]
72. Livak-Dahl, E.; Sinn, I.; Burns, M. Annual Review of Chemical and Biomolecular Engineering, Vol 2. Prausnitz, JM., editor. Vol. 2. Annual Reviews; Palo Alto: 2011. p. 325
73. Fuerstman MJ, Garstecki P, Whitesides GM. Science. 2007; 315:828. [PubMed: 17204610]
74. Rolland JP, Van Dam RM, Schorzman DA, Quake SR, DeSimone JM. J. Am. Chem. Soc. 2004; 126:2322. [PubMed: 14982433]
75. Ren KN, Dai W, Zhou JH, Su J, Wu HK. Proc. Natl. Acad. Sci. U. S. A. 2011; 108:8162. [PubMed: 21536918]
76. Begolo S, Colas G, Viovy JL, Malaquin L. Lab Chip. 2011; 11:508. [PubMed: 21113543]
77. Renckens TJA, Janeliunas D, van Vliet H, van Esch JH, Mul G, Kreutzer MT. Lab Chip. 2011; 11:2035. [PubMed: 21562649]

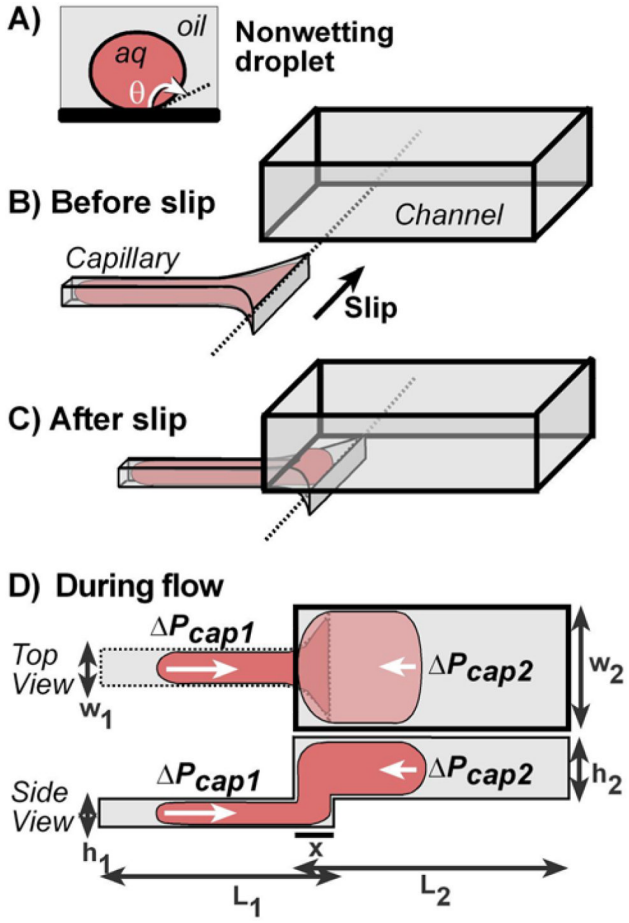

Figure 1.

Schematic drawings of the physical model and geometry used for capillary-pressure driven flow of a droplet from a "capillary" (smaller channel) to a larger channel on SlipChip. (A) The three-phase system, consisting of a nonwetting aqueous droplet (*red*) on a modified glass surface (*black line*), surrounded by immiscible oil (*grey*). The contact angle θ between the surface and the aq-oil interface is marked. (B,C) Three-dimensional schematics of a single capillary and channel on SlipChip. The capillary is in the bottom plate of the chip and the channel is in the top plate, so slipping the plates connects the capillary (pre-filled with aqueous solution) with the channel. (D) Two-dimensional top and side views, showing the capillary pressures (ΔP_{cap}, *white arrows*) for an aqueous droplet during flow.

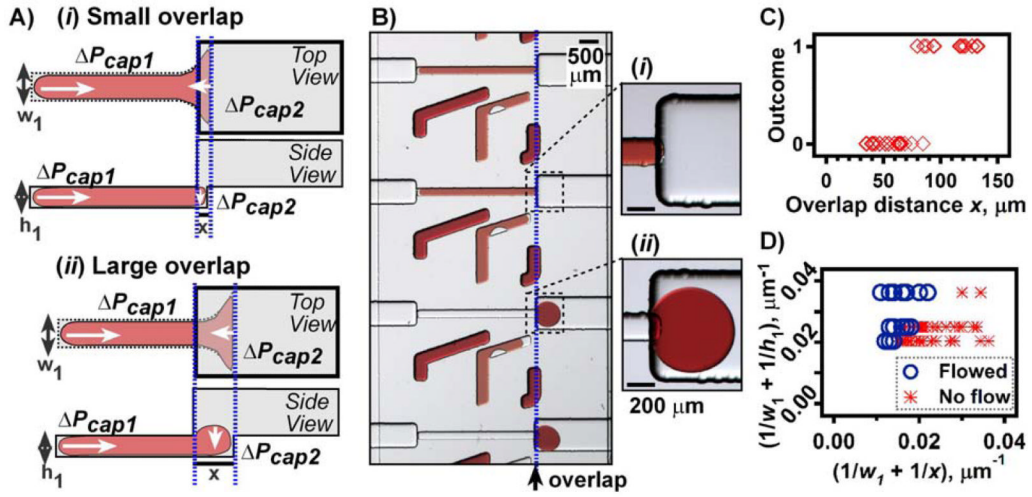

Figure 2.

Initiation of flow was controlled by capillary pressure at the overlap between the capillary and the channel. (A) Schematic drawings showing small (*i*) or large (*ii*) overlaps with length *x*. (B) Microphotographs of one portion a fluoro-silanized SlipChip after an initiation experiment. The capillaries were filled with a red aqueous solution and then slipped to overlap them with the channels. The region of overlap (*dashed blue line*) is expanded in the insets. Overlap length increased from top to bottom (x = 41, 65 (*inset i*), 94 (*inset ii*), and 132 μm), while capillary and channel depths were constant (h_1 = 50 μm, h_2 = 85 μm). No fluid flowed from the two top capillaries, while all fluid flowed from each of the two bottom capillaries into the channels to form circular droplets. (C) Plot of outcome versus x for chips with 50 μm deep capillaries (outcome 1 = flow, 0 = no flow; n = 4 trials). (D) "Phase diagram" plot of $(1/w_1 + 1/h_1)$ versus $(1/w_1 + 1/x)$, showing which size combinations led to initiation of flow. Blue circles indicate flow; red asterisks indicate no flow. n = 4 trials per chip.

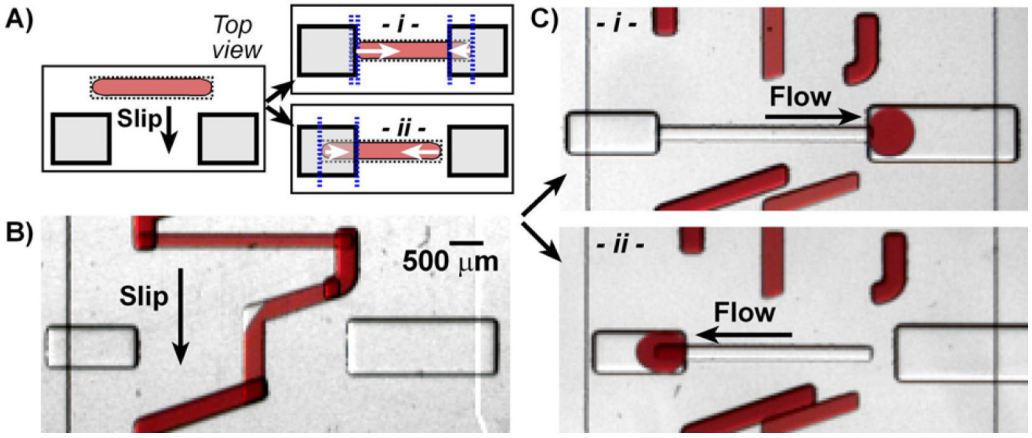

Figure 3.

Routing of flow by controlling the direction of slip and extent of overlap. (A) Schematic showing possible outcomes for flow, depending on the overlap between the capillary and channel. The capillary (*dashed line*) is in the bottom plate of the SlipChip. White arrows show capillary pressure, with the larger arrow indicating the predicted direction of flow. (B) A capillary in the bottom chip was filled with aqueous solution (red), then (C) slipped to into contact with either of the two receiving channels (*i*, *ii*). Flow was routed in either direction depending on the overlap with the channel.

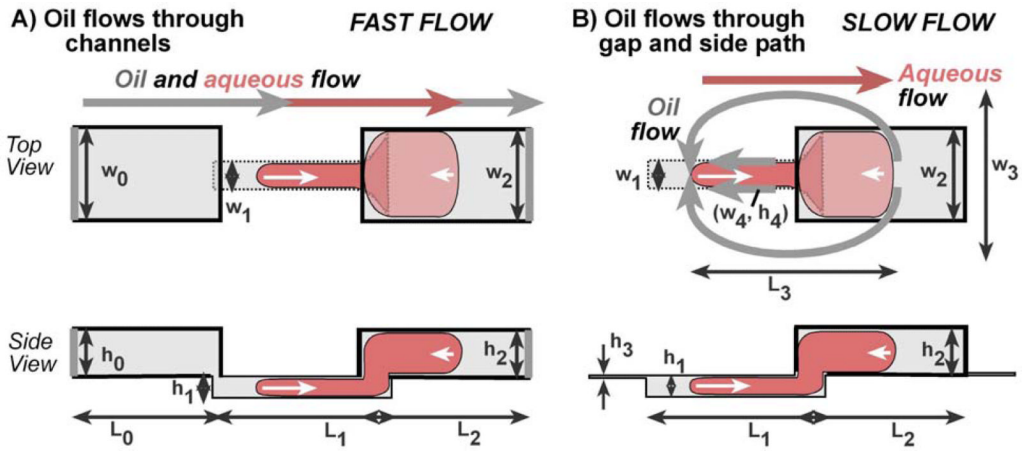

Figure 4.

Schematic drawings showing flow of aqueous droplets and oil through microfluidic channels. (A) Geometry with open reservoirs connected to the capillary and the channel for flow of oil. Pale gray lines indicate a fluidic connection to an open oil reservoir. Oil (*grey*) flows into the inlet channel at the left (dimensions w_0, h_o, L_0) and then into the capillary. Driven by capillary pressure (*white arrows*), aqueous solution (*red*) flows from the capillary into the receiving channel at the right, where it displaces oil into a second open reservoir. (B) Geometry without connected reservoirs. Gray arrows indicate the recirculation of oil through the gap between the plates of the SlipChip and through the sides of the capillary, driven by the flow of aqueous solution.

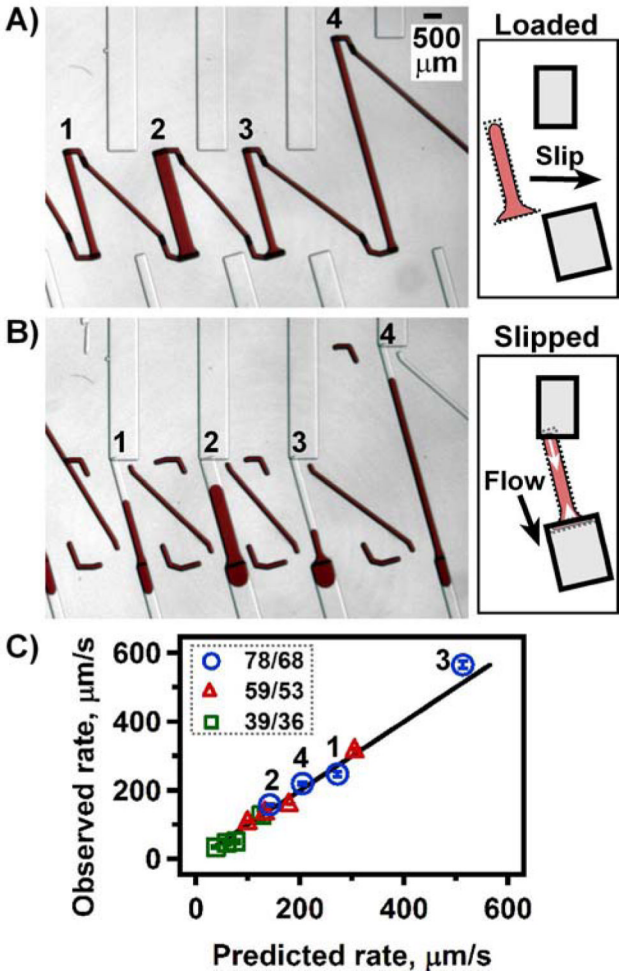

Figure 5.

Quantification of capillary-pressure driven flow rate (μm/s) on SlipChip and comparison to model predictions when oil flowed through channels. (A,B) Schematics and microphotographs of a SlipChip filled with aqueous solution (*red*), shown before slipping (A) and after slipping to the flow position (B). Each device had 4 conditions in duplicate, with varying widths and lengths of the capillary and channels (marked 1, 2, 3, 4). In the schematics, dotted lines indicate the bottom plate, while bold lines indicate the top plate. (C) Plot of observed versus expected flow rates in PDMS oil (55 mPa·s). Three depths of channels and capillaries were tested (channel/capillary depths given in legend, μm). Solid line shows the prediction. For the shallowest capillaries (green squares), the initial rates are shown. Error bars show one standard error of the mean (n = 8 data points, from 4 trials per chip).

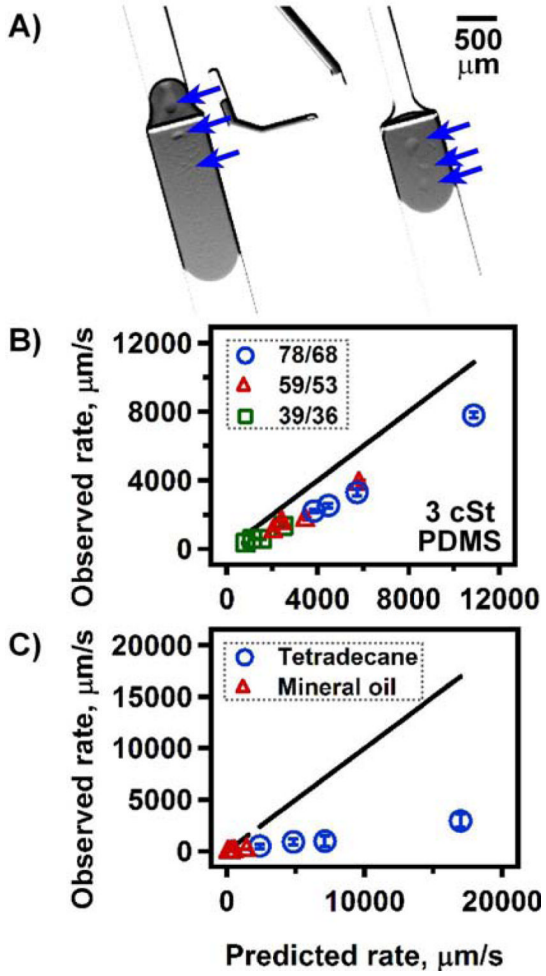

Figure 6.

Quantification of flow rates in systems where ruptured oil layers are hypothesized. (A) Microphotograph of aqueous droplets (*grey*) in 39/36 μm chip with 55 mPa·s PDMS oil. Rupture of the oil layer is suggested by observing droplets of oil (*blue arrows*) trapped under the aqueous droplets. The contrast and brightness of the image were increased to aid visualization. (B,C) Plots of observed versus predicted flow rate, μm/s, for droplets moving through (B) lowviscosity PDMS oil (2.8 mPa·s), or (C) hydrocarbon oils of low (2.1 mPa·s, tetradecane) or medium (21 mPa·s, mineral oil) viscosity. In (B), depths of channels and capillaries (μm) are given in the legend. In (C), only one depth (78/68 μm) was tested. Solid lines show predictions. Error bars show one standard error of the mean (n = 8 or 4-6 data points per condition for (B) and (C), respectively).

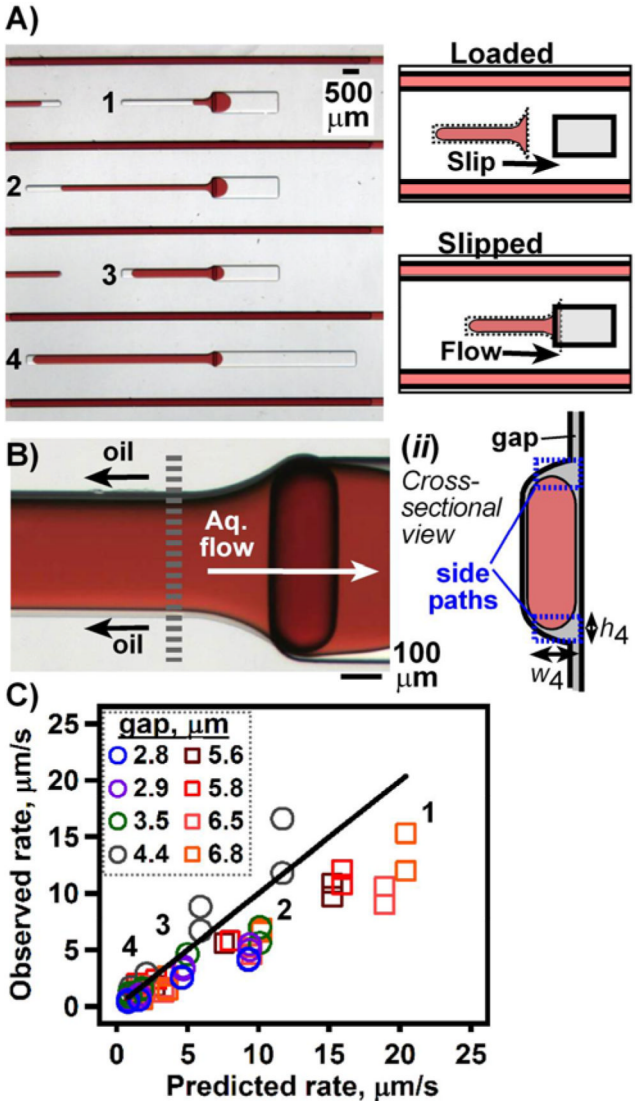

Figure 7.

Quantification of capillary-pressure driven flow rate on SlipChip and comparison to model predictions when oil flowed through the gap and side path (flow regime II). (A) Microphotograph of a SlipChip during flow, with schematics showing the chip before and after slipping to initiate flow. Each device had 4 conditions in duplicate, with varying widths and lengths of the capillary and channels (marked 1, 2, 3, 4). The red barriers between the channels were filled with aqueous solution to prevent motion of oil between capillaries. In the schematics, dotted lines indicate the bottom plate; bold lines indicate the top plate. (B) High magnification image of an aqueous droplet in a glass-etched channel during flow. The side path for oil is visible on each side of the droplet. *ii)* Schematic shows a cross-section of a droplet in a capillary. Blue boxes highlight the location of the irregularly shaped side path. (C) Plot of observed versus expected flow rates in PDMS oil (55 mPa·s). Several gap heights were tested (legend, μm) by using chips with 2 μm (circles) or 5 μm (squares) microposts. Solid line shows prediction

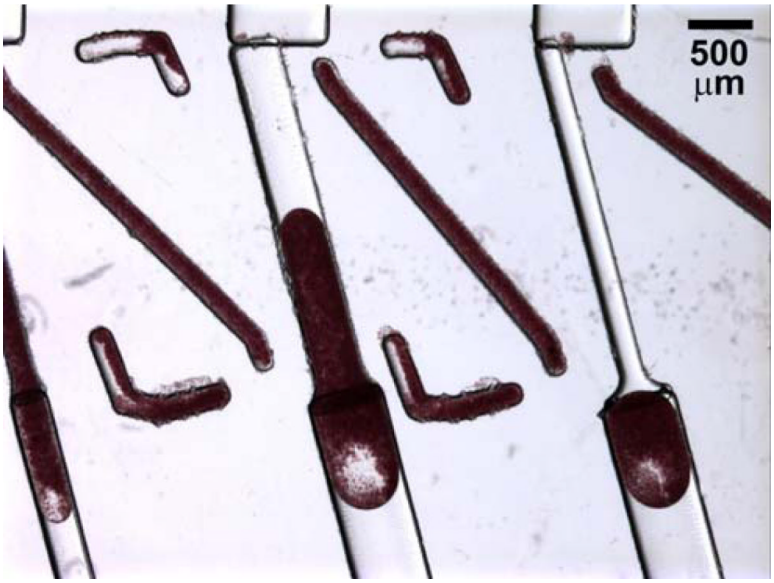

Figure 8.
Spontaneous, capillary-pressure driven flow of whole human blood on an FEP-dipped SlipChip. Microphotograph shows droplets of citrated whole blood, 10 sec after initiation of flow. The droplet on the right already finished flowing, while the flow of the left and center droplets was still in progress when the photo was taken. The carrier fluid was FC40 + 1 mg/mL RfOEG.